Eur. Phys. J. E (2019) **42**: 49
DOI 10.1140/epje/i2019-11812-1

THE EUROPEAN PHYSICAL JOURNAL E

Regular Article

Type-I collagen fibrils: From growth morphology to local order

Jean Charvolin and Jean-François Sadoc[a]

Laboratoire de Physique des Solides (CNRS-UMR 8502), Bât. 510, Université Paris-Sud (Paris-Saclay), F91405 Orsay cedex, France

Received 17 December 2018 and Received in final form 14 March 2019
Published online: 18 April 2019

Abstract. The length of type-I collagen fibrils in solution increases through the development and progress of pointed tips appearing successively at the two ends of an axis-symmetric shaft with constant diameter. Those tips, respectively fine (α) or coarse (β) have opposite molecular orientations. The α-pointed tips, the first to appear, are particularly remarkable as they all show, on most of their length, a common parabolic profile which stays constant during the growth. Assuming that the latter occurs by lateral accretion of individual molecules in staggered configuration, we propose to give account of this prominent morphological feature along a purely geometrical argument, the profile of a tip being linked to the shape of the trajectories followed all along the accretion process. Among several possible trajectories, Fermat spirals lead to a parabolic profile in perfect agreement with the one observed for α-pointed tips. This is to be put in relation with the presence of such spirals in phyllotactic patterns which ensure the best packing efficiency in cases of axis-symmetry, which is indeed that of dense collagen fibrils. Moreover, those patterns are structured by concentric circles of dislocations, constitutive of the structure itself, whose behaviour might contribute to the mechanical properties of the fibrils.

1 Introduction

Type-I collagen fibrils, cable-like associations of long biological molecules, the triple helices of tropocollagen, are the major constituent of connective tissues as different as, for instance, skin, bones, cartilage, tendons, myofibrils or cornea. The typical image of a fibril is shown in fig. 1.

Their length, several μm, is much larger than the constant diameter of their circular section, here 100–200 nm, they appear striated all along their length with a period $D = 67$ nm. These fibrils ensure the integrity of the tissues and are versatile enough to contribute to the wide variety of their specific functions. If this versatility is mainly driven by the physico-chemical nature of the environment, it also relies upon the adaptability of the fibril structure, or its mechanical compliance, to the stresses imposed by the variations of this environment.

The molecular organization of fibrils has been the object of many X-rays scattering studies during the last decades, the best information being obtained from rat tendon or lamprey notochord. They all show that the triple helices are densely aligned along the axial direction, at an intermolecular distance $d \approx 1.2$–1.3 nm, with a perfect translational order along this axis but not within the normal section. Although a local hexagonal packing is quite plausible in such a dense material, its long-range propagation may be questioned as the circular symmetry of the section is not strictly compatible with a crystalline order which would lead to a polygonal section[1]. Various models were developed to give account of these observations. However, without a clear understanding of the respective contributions of order and disorder to these data, it is difficult to discriminate among these models undoubtedly, as sketched in the appendix.

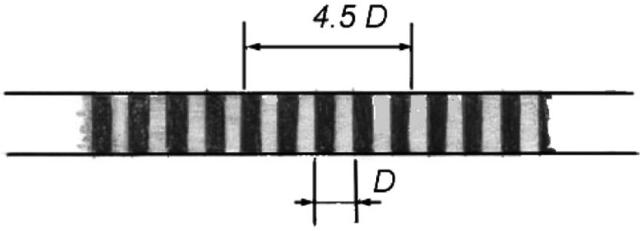

Fig. 1. Schematic drawing of part of a negatively stained type-I collagen fibril observed by electron microscopy, the striation period $D = 67$ nm and the length of one triple helix of tropocollagen is $4.5D$.

[a] e-mail: jean-francois.sadoc@u-psud.fr

[1] As, for instance, the hexagonal cross section of the large toroidal aggregates of DNA molecules hexagonally packed at an intermolecular distance of 2.8 nm [1].

We propose here to approach this structural question along a purely geometrical analysis based upon two firmly established elements of fibril description, at the microscopic and macroscopic scales, respectively (sect. 2). On the one hand, the geometry of triple helices interactions, as inferred from their chemical structure, on the other hand the morphology of growing fibrils. The lateral organization of triple helices, at midway between those two extremes scales, must bridge them coherently along a growth process by accretion respecting the circular symmetry of the normal section (sect. 3). This can be obtained organizing the triple helices along a self-similar phyllotactic pattern while the accretion progresses along the parastichies of the pattern[2] (sects. 4, 5). Phyllotaxis indeed ensures the best bidimensional packing possible in a situation of circular symmetry at the price of positional disorder and self-similar ordering of dislocations concentrated along concentric circles of increasing radii. The first contributes to the disorder observed in the normal section and the second might favour original mechanical behaviors (sect. 6).

2 Descriptive data

2.1 At the microscopic scale: staggering of triple helices

Triple helices have a length $L = 300\,\text{nm}$, a diameter of 1.1 nm and the X-ray scattering data show that they are densely packed at an average distance d of at most 1.3 nm. The striations with a period of 67 nm observed all along the fibrils by electron microscopy led to propose the staggered molecular organization of fig. 2 [2–8].

This drawing, which has become a standard, conveyed the idea that such bidimensional sheets, with strong intermolecular interactions, might be the elements whose assembly, with weaker interactions, builds the fibril. However the association of bidimensional sheets in the tridimensional structure of an axisymmeric fibril proved to be problematic. Several models have been examined which are recalled in [9–11], but the complexity of the information provided by X-ray scattering data does not help to choose between them definitively (see the appendix). Broadened peaks merging out from a very important and variable background scatter suggest that the molecular organization in the fibrils cannot be related to classical ones such as molecular crystals, whose tridimensional order would be perturbed by external constraints or thermal disorder, or liquid crystals of long molecules aligned along a common direction, with a liquid disorder in the normal plane. We shall consider that the bidimensional sheet of fig. 2 builds itself as the accretion progresses along a trajectory, which is a constant compromise between density and symmetry constraints.

[2] The classical example of a phyllotactic pattern is that shown by a sunflower head, the parastichies are the quite visible spirals drawn by the florets.

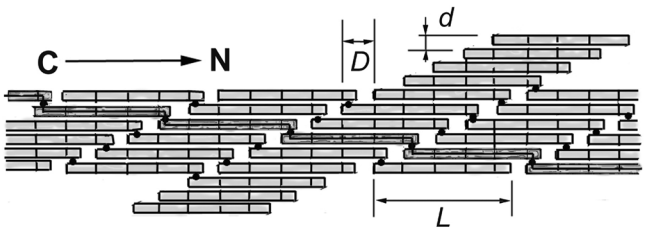

Fig. 2. Interactions between segments of triple helices, particularly a strong head-tail cross-linking (black dots), determine the $1D$ staggering responsible for the axial striations with period $D = 67\,\text{nm}$ of the fibrils. The molecules are also often represented as arrows from their C to N terminal telo-peptides. In black a filament of molecules with $4D$ stagger (see sect. 3).

2.2 At the macroscopic scale: morphology of growing fibrils in solution

The very first steps of the formation of type-I collagen fibrils in solution are diversely described; most likely they depend upon the origins of the triple helices and the conditions of their associations [12–19]. Those steps are generally considered as providing precursory aggregates for the growth to be considered in some details later (sect. 3). Once those steps are passed over, a single description stands out [20, 21]:

- lateral and axial growth proceed simultaneously, the first being constrained to stay within a given diameter (owing to double twist [22–24] and surface tension [24, 25], a mechanism which we do not consider here[3]) while the length increases;
- the two ends of this growing object differ, one, a blunt or frayed end, is first inactive and the elongation takes place on the other via the development of a fine α-pointed tip with a constant parabolic profile on most of its length, its triple helices being directed towards the end of the tip;
- eventually, later, the blunt end can become active developing a shorter coarse β-pointed tip with a less well-defined parabolic shape, the orientation of its triple helices being opposite to that of the α-pointed tip;
- the zone where the orientation of the triple helices turns over is visible along the shaft, most likely close to where the blunt end was.

The fact that this elongated object stays axis-symmetric, in its pointed tips as well as in its shaft, implies that the molecular accretion during the growth proceeds accordingly.

This process and the unipolar or bipolar fibrils thus formed are sketched in fig. 3. Those observations concern a first stage of the growth, where the diameter stays limited to about 100 nm (larger fibrils, whose section may

[3] With a double twist of pitch P the molecules are tilted with respect to the fibril axis by an angle $\Phi_x = (2\pi/P)x$ along its radius and the profile of the tip calculated below will have to be multiplied by $\cos\Phi_x$, but, with $P = 2400\,\text{nm}$ (see [23]) and $x = 50\,\text{nm}$ (the fibrils considered here), $\cos\Phi_x \approx 0.993$, *i.e.* a relative variation of 7.10^{-3} which can be neglected.

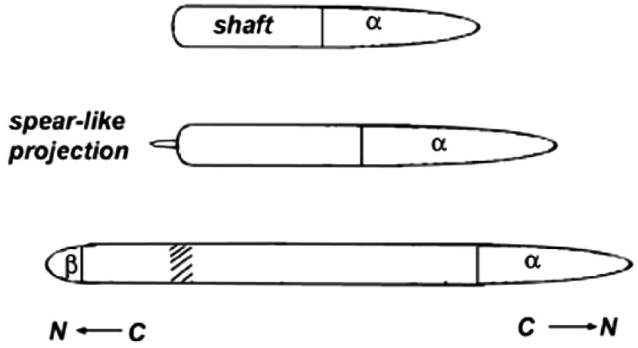

Fig. 3. A unipolar then bipolar axis-symmetric fibril, the hatching on the second represents the zone where the orientation of the triple helices turns over. The ratio between diameter (of the order of 100 nm) and length (several tenths of μm) is not respected.

appear rather irregular in shape, were suggested to be associations of smaller fibrils [26]).

The parabolic shape of a pointed tip was deduced from the linear behavior of its mass per unit length m_l as the distance y to its end increases, as shown in fig. 4 [26–28]. Indeed, if the shape of a tip is that obtained rotating a parabola $y = ax^2$ around its y-axis, its mass per unit length m_l varies as $m_l = \rho\frac{\pi}{2a}y$, ρ being here the density of the STEM image calculated from the mass of a triple helice, 290 kDa, and using a TMV virus as a mass standard [27].

The fine α-pointed tips exhibit a common regular linear evolution of m_l on most of the length studied (fig. 4(a)). This is not the case for the coarse β-pointed tips whose less regular evolutions of m_l vary within a rather large extent (fig. 4(b)). Whereas the α-pointed tips have a common average slope $\rho\pi/2a \simeq 0.2\,\mathrm{kDa/nm^2}$, the β-pointed tips are distributed between 0.74 and 2 $\mathrm{kDa/nm^2}$. Moreover, for α-pointed tips, departures from linearity occur at the two extremes of the plots: when approaching the central shaft and, in a few instances, in the immediate vicinity of the tip end. These departures from linearity share in common the fact that any overall curvature in the curve is downward, never upward [27]. Parabolic profiles are therefore certain for portions of the α-pointed tips having a length of about 8 μm only.

Finally, a morphology related to that of a bipolar fibril was observed for fibrils of type-II procollagen, but the profiles of the two pointed tips are identical and their molecules are oriented the other way round in both pointed tips [29].

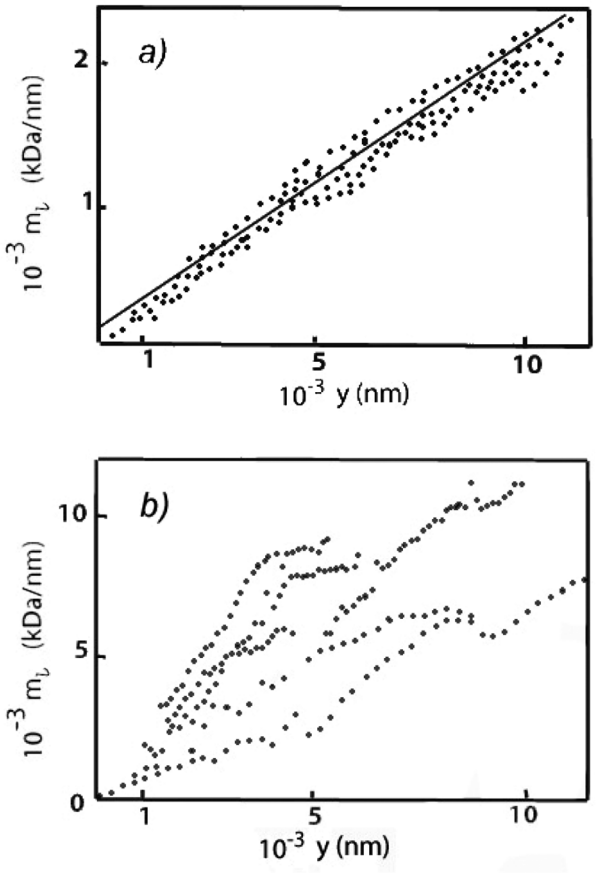

Fig. 4. Behaviors of the mass per unit length m_l for several α-pointed tips (a) and β-pointed tips (b) as the distances y from the ends of the tips increase, the straight line in (a) is obtained by a least-square fit, from [27].

3 Accretion

3.1 Accretion around a precursor

As announced in sect. 2.2 the growth of striated collagen fibrils is anticipated by the formation of elongated thin aggregates of parallel molecules which constitute precursory aggregates for the growth. Those precursors with widths from a few nm to at the most 20 nm do not present, for most of them, the striation with period $D = 67$ nm. Two studies [16, 17] indeed observed that procollagen molecules, which will be transformed into tropocollagen ones later, build slender "segment long spacing" (SLS) aggregates of parallel molecules without staggering which, in turn, associate end to end in long filaments incorporated into growing striated fibril of staggered molecules[4]. Also, a study of the structure of fibril components present in solution [30] concludes that linear filaments of molecules with predominant $4D$ stagger, as the black line in fig. 2, are a particularly stable form of aggregation in solution which could be seen as basic units of the fibrillar structure. Finally, as reported in sect. 2.2, the fact that the growing fibril stays axis-symmetric enables one to suppose that the growth respect this symmetry, starting all around the precursor at a defined level O of it.

Those three observations lead us to build a growth model following which a precursor of finite width and SLS organisation, be covered in successive steps by molecules optimizing their interactions at every step as sketched in

[4] Inversely, short SLS segments with one molecular length can grow on a long striated fibril [2].

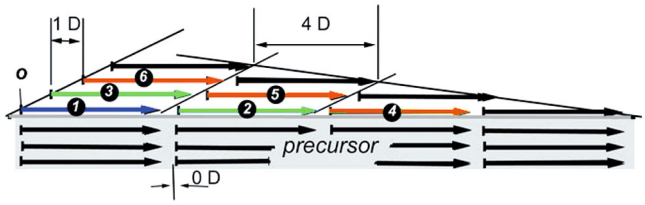

Fig. 5. Accretion of triple helices from level O of a precursor in SLS configuration, layer after layer of triple helices in $4D$ stagger, the maximal covering of new triple helices over previous ones result in a $1D$ stagger at the initial point of accretion and a $4D$ stagger at the opposite end where growth occurs. A new triple helix at a given level, must stand on two triple helices of the previous level: "3" must wait that "2" has been placed, then after that, the only one possibility is to place "4" and so on. As in fig. 3, the ratio between diameter and length is not respected.

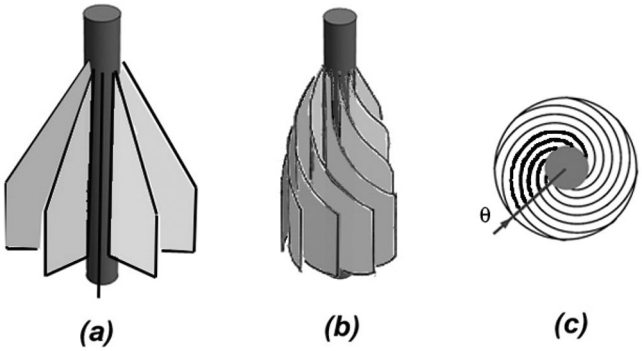

Fig. 6. Wrapping up around the precursor of the radial trajectories of (a) into spiral ones (b), the spirals seen from above in (c), in bold the parts of their arms to be considered to calculate the profile along an arbitrary radius at θ (c).

figs. 5 then 6. This view presents a similarity with that of a previous model based on diffusion limited aggregation [31]. Once the first molecules are anchored around the precursor at level O (step 1), a layer of two molecules thick would built itself around the precursor (step 2) and the first anchored molecules (step 3), then a layer of three molecules thick around the previous one (steps 4, 5, 6) and so on. Thus, the fibril grows laterally and axially but, owing to the fact that the lateral growth is limited, an aggregate is formed having a cylindrical shaft with constant diameter ended by pointed tips with $4D$ and $1D$ staggerings, respectively, the first being the site where the growth takes place.

3.2 Accretion trajectories

As accretion progresses from the surface of the precursor to the periphery of the growing fibril, the trajectories followed must be compatible with the circular symmetry and a density as constant as possible. The most regular trajectories, without abrupt fold, can be radial, spiral or circular.

Radial trajectories radiate around the axis, as shown in fig. 6(a), they diverge and the density of triple helices can only be maintained introducing more and more trajectories between the first ones as the radius increases, each new one corresponding to an edge dislocation. The geometry of such a configuration leads to conical pointed tips as the positions of the molecular ends in fig. 5 vary linearly with their distance to the axis.

Spiral trajectories appear quite liable to build dense non-conical pointed tips. The rolling up of the radial trajectories of fig. 6(a) sketched in fig. 6(b) brings, according to the spiral chosen, the opportunity for several possible variations of the positions of the molecular ends as function of their distance to the axis, while avoiding the radial divergence. The profile along an arbitrary radius of given θ is obtained multiplying the amplitude of one step of staggering by the number of staggerings along each spiral arm from the precursor to its intersection with the radius, as shown in fig. 6(c). As the growth starts on a precursor of radius r_p, density and circular symmetry require the anchoring of $k = 2\pi r_p/d'$ spiral trajectories, d' being their distance at its periphery, *i.e.* a multistart spiral with k arms.

Circular trajectories have also been proposed assuming that the fibril is built by successive cylindrical sheets of one molecular thickness, the end of each one being shifted by $4D$ with respect to the previous one [32]. This geometry also leads to conical pointed tips as the profiles of the successive shifts vary linearly with their distance from the axis. However, parabolic profiles could be obtained attributing different molecular binding constants within each sheet, with $1D$ staggering, and between two adjacent sheets, with $4D$ staggering.

4 Spirals for α-pointed tips

Among many types of possible spirals, we choose to compare the two which are most liable to maintain a constant density, the two for which the distance between consecutive turns does not increase with the azimuthal angle. One is the Archimedean spiral $\rho = a\theta$ with a constant distance $2\pi a$ between its turns, the second is the Fermat spiral $\rho = a\sqrt{\theta}$ whose distance between turns decreases, but very slowly on a rather large variation of θ.

4.1 Archimedean multistart spiral

A multistart spiral with k arms is a set of k spirals each deduced from the Archimedean spiral $\rho = a\theta$ by a rotation of angle $\phi_n = 2\pi n/k$, with n from 0 to $k-1$. Each arm bears a succession of points at the intermolecular distance d and the average distance between two arms n and $n+1$ is chosen as $2\pi a/k \approx d'$ with $d' \approx d\sqrt{3}/2$ in order to simulate a dense hexagonal local packing. As sketched in fig. 6(c) each of those spirals intersect a radius for instance $\theta = 0$ (all are equivalent owing to the circular symmetry) at a distance $\rho_n = 2\pi an/k$ after having run over a length $L_n(\phi_n) = \frac{a}{2}[\phi_n\sqrt{1+\phi_n^2} + \ln(\phi_n + \sqrt{1+\phi_n^2})]$ from the origin. Each point on the spirals corresponding to a down

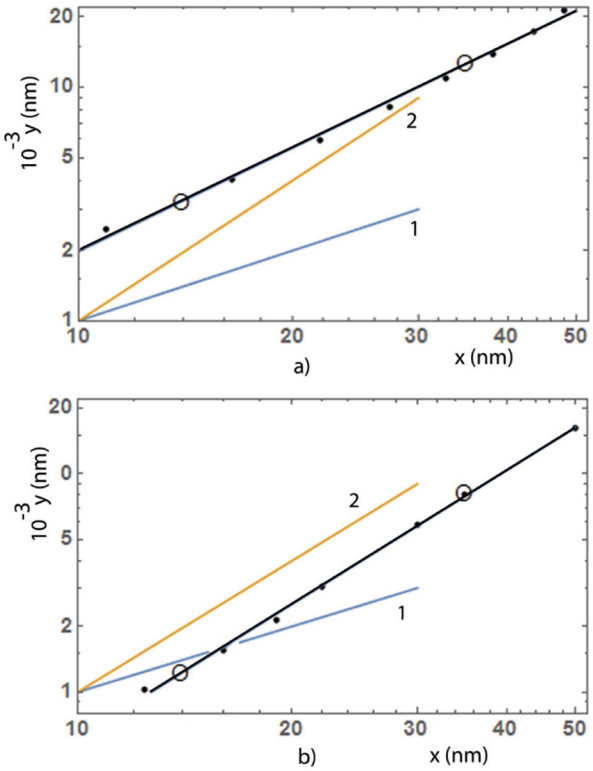

Fig. 7. Log-Log plots of the profiles obtained with the multistart Archimedean spiral $k = 80$ (a) and the (89) family of parastichies (b), the slope of the first is $\cong 1.4$, that of the second is 2, the circles corresponds to the limits, from $x = 14$ nm to 35 nm, of the drawing of fig. 5 in [28], thin colored lines corresponds to slopes 1 or 2.

step of height $4D$, as in fig. 5, the evolution of the profile along a radius from the precursor of radius r_p is then given by $y_n = \frac{4D}{d} L_n(\phi_n)$ as a function of $x_n = a\phi_n = \rho_n$.

Assimilating the precursor with the linear initial aggregates observed before lateral growth [2,15], which have in majority a radius of 13 nm similar to the minimal radii 14 nm of the reconstitutions of parabolic profiles in [28], we use the value $k = 80$, deduced from $k = 2\pi r_p/d'$ with $r_p \approx 14$ nm, k being also $2\pi a/d'$, to calculate the profile represented by the Log-Log plot of fig. 7(a).

The Log-Log plot of the profile built by the Archimedean multistart spiral having a slope $\neq 2$, this profile cannot be a parabola. Moreover, the length of the portion of pointed tip in between radii of 14 nm and 35 nm deduced from this curve, 11.6 μm, is not in agreement with the one, 6.7 μm, measured in [28].

4.2 Fermat spiral of phyllotaxis

Phyllotaxis has been shown to provide the best packing efficiency, as far as isotropy and homogeneity are concerned, for situations of circular symmetry or with circular confinement [33]. We recently proposed that the self-similar lateral organization drawn by the algorithm of phyllotaxis, with an intrinsic coexistence of order and disorder, might

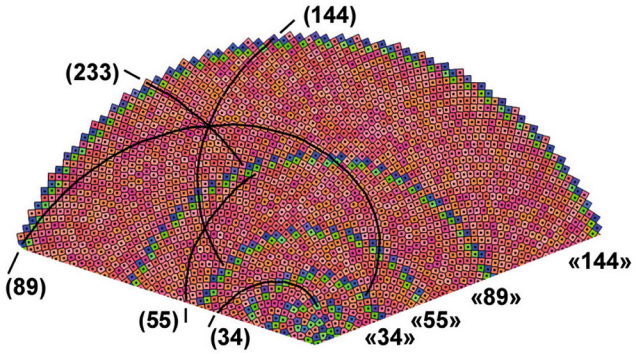

Fig. 8. A sector of a pattern of 6500 points organized according to the algorithm of phyllotaxis with the golden ratio, the radius of this sector is 52.4 nm, each point is surrounded by its polygonal Voronoi cell whose number of sides corresponds to the number of first neighbors around this point, blue cells are pentagons, red cells hexagons and green cells heptagons, those polygons are not necessarily regular, grain boundaries and members of the families of parastichies are identified as $\ll n \gg$ and (n) respectively.

contribute to the complexity shown by X-ray scattering studies of collagen fibrils [11]. A sector of a phyllotactic pattern is shown in fig. 8, such a pattern having been analyzed in details from a purely crystallographic point of view in [34].

In such a Voronoi pattern, pentagons and heptagons are topological defects distributed among a majority of hexagons. They appear concentrated in narrow circular rings with constant width separating large rings of hexagons whose width increases from the core towards the periphery. In the narrow rings, pentagons and heptagons are associated in dipoles which could be considered as dislocations in a hexagonal tiling. These topological defects are needed to ensure a density as constant as possible [34]. Those rings can be seen as grain boundaries, identified by their number of dipoles $\ll n \gg$, separating hexagonal grains. In each hexagonal grain three families of lines, the parastichies, join first neighbor points, each family being identified by its number of parastichies (n). Those parastichies, which can be seen as the reticular lines of a bidimensional bent lattice of the pattern, are the Fermat spirals examined here as eventual accretion trajectories.

In this pattern, and from the radii evaluated by the measurements of [27] and [28], the zone of the latter would correspond to the three hexagonal grains limited by grain boundaries $\ll 34 \gg$ and $\ll 144 \gg$, the families of parastichies present in this zone being classified in table 1.

One family of parastichies, (89), passes through the three grains along which the profile can be easily determined counting the number of points on each parastichie of the family from grain boundary $\ll 34 \gg$ to an arbitrary radius and attributing a down step of $4D$ from point to point. The Log-Log plot of the profile so obtained is represented in fig. 7(b), it has a slope of 2, this profile is therefore parabolic and is described by the equation $y = 6.5x^2$. From this equation, the length of the portion of parabola in between radii 14 nm and 35 nm is 6.7 μm, a value which

Table 1. Parastichies in the zone of interest (grey columns) and its immediate surroundings, the grain boundaries are identified by their numbers of dipoles and the three families of parastichies in each hexagonal grains are identified by their numbers of parastichies, those numbers are Fibonacci's numbers.

Grain boundaries	$\ll 21 \gg$		$\ll 34 \gg$		$\ll 55 \gg$		$\ll 89 \gg$		$\ll 144 \gg$		$\ll 233 \gg$
Radius (nm)	7.7		12.4		20.1		32.5		52.4		84.8
Families		(21)		(34)		(55)		(89)		(144)	
of parastichies		(34)		(55)		(89)		(144)		(233)	
in grains		(55)		(89)		(144)		(233)		(377)	

agrees well with the one reported in [28]. Also, the slope of m_l as function of y, $\rho\pi/2a$, is $0.18\,\mathrm{kDa/nm^2}$, a value quite close to the one, 0.2, measured on fig. 4(a).

Thus, the family of parastichies (89) leads to a profile in quite good agreement with the observed one. The preference for this family over the two others also present in the first grain, (34) or (55), holds to the fact that the number of trajectories anchored on the precursor, 89, is close to the estimation of this number, $k \approx 80$, made in sect. 4.1.

4.3 Range of validity

As mentioned in sect. 2.2, m_l as function of y departs from linearity with downward curvatures as the two extremes of the plots are approached [27]. The family of parastichies (89) being no longer present in these regions it is tempting to follow the same step than above with families (21), (34) or (55) close to the tip end, and (144), (233) or (377) close to the shaft. However, only upward curvatures can be obtained as the slope steadily increases with the number of parastichies in a family, for instance: $0.13\,\mathrm{kDa/nm^2}$ for (55), 0.18 for (89), 0.33 for (144) and 0.45 for (233).

Most likely, as proposed in [27], the decrease of the slope observed at large distances from the end of the tip should be related to the fact that m_l tends to be constant as the cylindrical shaft, with a diameter around 100 nm, is approached. On the other hand, the rapid decrease of m_l observed for certain fibrils when approaching the tip end occurs at a distance of about $1.3\,\mu$m [27,28] where the radius would be 14 nm, the value at which the anchoring of the accretion trajectories on the precursor occurs, *i.e.* a region unsufficiently described to go further.

Two remarks can be made about each of these points. One is that the fibrils studied here [26, 28] keep a constant diameter all along the growth, notwithstanding the fact that fibrils with larger diameters have been observed in tendons. If it was suggested, as alredy said, that this might result from aggregation of those fibrils [26], another eventuality might also be the triggering of a new stage of growth by accretion of triple helices around them along new parastichies. The second remark concerns the fact that mathematical phyllotaxis is usually developed from a central point rather than around a precursor with a finite radius. This should not be redhibitory as, in botany, similar phyllotactic patterns can be observed around various apical meristem profiles and radii [35] and as the development of a pattern was shown to be insensitive to perturbations within its core such as anihilation or creation of cells [36].

5 Extension to β-pointed tips?

Those tips appear shorter than α-pointed tips [27,28], this suggests that the staggering of their triple helices is not $4D$ but most likely its complement $1D$. This would be the case if the growth of the β-pointed tip was to occur on the end with $1D$ scattering of fig. 5, left inactive up to now. If this was the case and if the accretion trajectories were still along the parastichies of family (89), the slope of the mass m_l per unit length of the tip as a function of y should be four times that of the α-pointed tip, *i.e.* 0.8, while the linear approximations of the curves in fig. 4(b) show slopes varying from $0.74\,\mathrm{kDa/nm^2}$, close to 0.8, up to 2.

Most of those slopes being higher than $0.8\,\mathrm{kDa/nm^2}$, other families of parastichies than (89) might be considered, for instance (144) would give a slope of 1.34 and (233) a slope of 1.82. Following what was said in 4.2 about the relation between the number of trajectories anchored on the precursor and its radius, the precursors should therefore have respectively the radii of grain boundaries from which they start, $\ll 55 \gg$, 20 nm, and $\ll 89 \gg$, 32 nm, from table 1. It is then tempting to put this in relation with the observation prior to the growth of the β-pointed tip [20] of a spear-like projection out of the blunt end having a larger radii than the precursor. However, owing the present state of the description of this growth, it is too detailed a speculation to go any further.

Several questions raise at this stage: does the precursor evolves after accretion, what is hidden behind the terms of blunt or frayed end, where does the spear-like projection comes from and where does it go, how turned over triple helices can interact with the blunt end in the reversal zone?

6 Summary and prospect

Measurements made on α-pointed tips of several growing fibrils, on a length of about $12\,\mu$m from the end of the tip, reveal that, on a large part of this length, $7\,\mu$m, those tips exhibit a common parabolic profile which stay constant

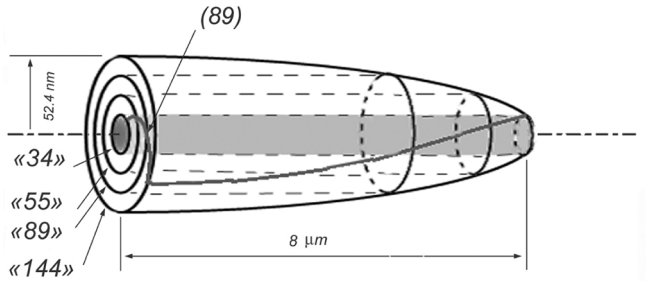

Fig. 9. The paraboloidal portion of a α-pointed tip with, in section the precursor (grey), the concentric grain boundaries which are directors of cylinders of dislocations extending all along the fibril, the Fermat spiral of one parastichy of the (89) family and its trace on the surface, once again the ratio between diameter and length is not respected.

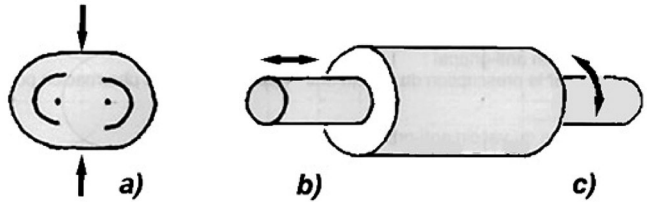

Fig. 10. Flattening of a circular section accompanied by the splitting of a circle of dislocations in two half circles (a), relative motions of hexagonal grains separated by a cylinder of dislocations would be made possible by the weakening of interactions along the latter (b), (c).

as the growth proceeds. In an attempt to give account of this behavior we examined the geometry of a tip which would be built wrapping up accretion trajectories of staggered triple helices around a precursor of constant radius. The parabolic profile obtained this way, and its extension along the α-pointed tip, are in quite good agreement with those observed if the trajectories are aligned along one family of parastichies of phyllotaxis. The volume of staggered triple helices surrounding the precursor in the domain of the measurements is schematized in the drawing of fig. 9.

Beyond our morphological point of view, the functionality of such a complex organization should be questioned. Collagen fibrils being, most often, cable-like structuring materials of organisms, this concerns their behavior under external constraints. Concentric cylinders of dislocations, orientations of the parastichies relative to them and the reversal zone in bipolar fibrils are liable to contribute to mechanical properties, as sketched in fig. 10:

- motion of dislocations under deformations of the circular section of a fibril by a localized lateral pressure, or by a pronounced bending, as observed in [37], could contribute to the bending strength of the fibril;
- parastichies (89) ending on grain boundary $\ll 144 \gg$, a new stage of growth must follow parastiches with different orientations, the lateral interactions between triple helices are interrupted and the interactions between the two grains on either sides of this grain boundary could be weakened affecting the bending or torsional strengths;
- the diversity of β-pointed tips lets suppose a comparable diversity of interactions between triple helices with opposite orientations in the reversal zone, this should affect the tensile strength.

7 Conclusion

A little more than 50 years ago, the first studies of type-I collagen fibrils by electron microscopy put in light the great originality of their cable-like morphology. This gave rise to a series of structural investigations, mainly X-ray scattering studies, which, in turn, triggered the development of various models, each one bringing a new perspective about the lateral order of long biological molecules in those fibrils. However, each time a new, but never definitive perspective, owing to the difficulty to analyze the data collected with the usual concepts of condensed matter physics.

Considering that the circular symmetry of the fibril is not compatible with any crystalline order, we therefore proposed to describe the lateral packing of collagen fibrils with the algorithm of phyllotaxis which builds the best dense axis-symmetric packing possible by substituting an original inflation-deflation symmetry to the translational and rotational symmetries of classical crystallography. Although this approach gave account of the available data in a somewhat satisfactory manner, as the previous ones succeeded to do, the agreement obtained is not strong enough to give it a particular primacy over others at this stage. This led us to consider the original and well-documented growth morphology of the fibrils, expecting that it would be possible to deduce from it an argument in favor of our proposal. It indeed appeared that a growth along the parastichies of phyllotaxis by accretion of collagen molecules in staggered configuration builds end tips of fibrils with a parabolic profile similar to the one measured. This leads to two concluding remarks.

First, this work takes part in the actual interest for packings of long biological molecules in cable-like structures with diversified behaviors adapted to various functionalities in organisms. The description of those dense molecular assemblies is made complex by the fact that they are submitted to geometrical frustrations which prevent the propagation of any long-range order and impose the presence of structural defects. We see two major causes of frustrations in those systems. One is the search for a circular normal section under interfacial tension, treated here calling for the algorithm of phyllotaxis in the particular case of staggered collagen molecules. The other is the double twist configuration imposed by molecular chirality, the solution was examined alone, as well as coupled to the previous one, for ideal smooth molecular filaments [25,38]. In both cases the defects needed to relax those two frustrations are identified and localized. They build dislocations which can be organized radially, circularly or radially beyond a critical radius. Such analysis should contribute

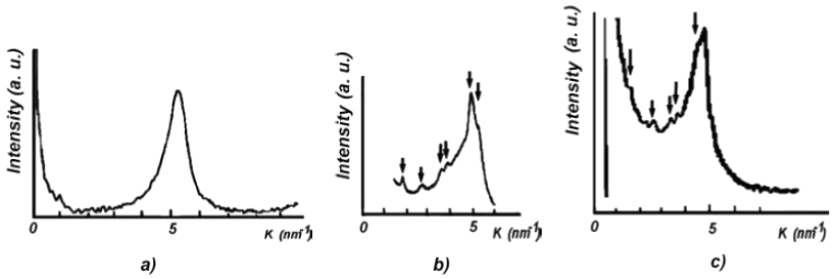

Fig. 11. Raw X-ray scatterings along the direction normal to fibril axes in native tendons: (a) from [42]; (b) from [9] and (c) from [43].

to the understanding, not only of fibril morphologies, but also of their behaviors under mechanical constraints, one aspect of their functionality.

Second, the simple algorithm of phyllotaxis, describing vegetal growths on a macroscopic scale by addition of successive florets at the center of flowers, the oldest being pushed aside by the new ones, is here proposed to describe a growth on a microscopic scale proceeding the other way round, molecules being successively added around a central core. Because of those two differences, macro or microscopic scales and growth from the inside or the outside, collagen fibrils would correspond to a new situation. If other modalities of formation of phyllotactic spiral organizations are recorded (Bénard-Marangoni convection cells in a liquid layer contained in a cylindrical container and submitted to a vertical temperature gradient [39], distribution of ferrofluid droplets falling down in a silicone oil in presence of a vertical inhomogeneous magnetic field with cylindrical symmetry [40], bubbles on a circular water surface [41]), they all develop themselves on macroscopic scales and not by accretion from the outside. Type-I collagen fibrils would therefore appear as an original example of a growth by accretion along phyllotactic spirals on a microscopic scale which suggests similar investigations on other dense fibrous proteins, keratin or collagens without striations such as cuticular ones for instance.

Appendix A. X-ray scattering studies

The lateral packing of triple helices in a fibril was mainly investigated by X-ray scattering studies. Three examples of scattering intensity curves observed along a normal to the fibril axis are displayed in fig. 11. These are raw data [9,42,43], without any treatment to isolate the small discrete maxima from the background. They all exhibit a strong intensity maximum at $k = 5\,\mathrm{nm}^{-1}$ and, eventually, small discrete maxima at lower k values merging out from an important background scatter. This suggest that the molecules are densely packed in a somewhat ordered manner, but the breadths of those maxima and the presence of an important background scatter exclude the possibility of a strict bi-dimensional crystalline order.

Various models were developed to give account of those intensity curves. Most of them are analyzed and their Fourier transforms compared with experimental data [9]. The number of those models illustrate the difficulty for approaching the very nature of such data, particularly as far as the origin of the disorder is concerned. We choose some of them which, in our point of view, correspond to different conceptual steps.

The so-called "quasi-hexagonal" model of [44] consisted in searching for how a simple hexagonal lattice, with an intermolecular distance deduced from the maximum at $k = 5\,\mathrm{nm}^{-1}$, should be deformed to give account of the positions of the maxima observed at lower k values. A correct fit was obtained with a monoclinic unit cell. It was suggested that the breadth of the maxima might result from fluctuations of the unit cell content and the background scatter from a disordering of some fibrils or part of fibrils. A development of this model consisted in showing that super-twisted microfibrils of five triple helices, assembled along the quasi-hexagonal cell, can interdigitate to build a compact ordered fibril [45]. Those models do not take the constraint of circular symmetry into account.

This symmetry was simulated placing angular sectors with quasi-hexagonal order side by side around the fibril axis [9]. The position of one out of five triple helices being vacant, as required by the staggering of fig. 3, with a specific ordering by groups of five. The disorder is localized in the radial grain boundaries between sectors and around the axis. This model accounts for both the intensity maxima, their breadths and the background scatter in a situation approaching circular symmetry.

The spectrum of fig. 11(a), showing only one broad intensity maximum, is a particular case which was analyzed within the the frame of the paracrystal concept [42]. The relative positions of triple helices are not derived from a hard-core potential but from a one-parameter distribution function characterizing the propagation range of a local hexagonal order. There is no long-range order in this model and the calculated shapes of scattered intensity are in good agreement with this particular spectrum.

In those three models, monocrystalline, polycrystalline and paracrystalline, the fibril is looked at as a classical molecular crystal in which disorders of different natures are purposely introduced: defects in fibril configuration, grain boundaries or mathematical function. Their disorders can be said extrinsic. Conceptually different models, in which the disorder is intrinsic, not imposed to the structure but constitutive of the structure itself, have been also considered.

The first attempt consisted in examining aperiodic square-triangle lattices built applying the inflation-deflation procedures developed for quasi-crystals. The triple helices have here six or five first neighbours at a constant intermolecular distance. Such lattices have no unit cell with long-range order as in a crystal, the intermolecular contacts with topological disorder are uniformly distributed throughout in a self-similar manner, as in a quasi-crystal. The Fourier transform show broadened peaks whose positions are in rather good agreement with those of the maxima observed [46].

The organization of triple helices along a self-similar phyllotactic pattern discussed here indeed belongs to this class of structures with intrinsic structural disorder.

Author contribution statement

JC and J-FS contributed equally to the research, to the analysis of the results and to the writing of the manuscript.

References

1. A. Leforestier, F. Livolant, J. Mol. Biol. **396**, 384 (2010).
2. A.J. Hodge, F.O. Smith, Proc. Natl. Acad. Sci. U.S.A. **46**, 186 (1960).
3. A.J. Hodge, J.A. Petruska, in *Aspects of Protein Structure*, edited by G.N. Ramachandran (Academic Press, New York, 1963).
4. J.A. Petruska, A.J. Hodge, Proc. Natl. Acad. Sci. U.S.A. **51**, 871 (1964).
5. J.W. Smith, Nature **219**, 157 (1968).
6. J. Woodhead-Galloway, Acta Crystallogr. B **33**, 1212 (1977).
7. A.L. Bailey, N.D. Light, E.D.T. Atkins, Nature **288**, 408 (1980).
8. J.P. Orgel, T.J. Wess, A. Miller, Structure **8**, 137 (2000).
9. D.J. Hulmes, T.J. Wess, D.J. Prockop, P. Fratz, Biophys. J. **68**, 1661 (1995).
10. D.J. Hulmes, J.-C. Jesior, A. Miller, C. Berthet-Colominas, C. Wolff, Proc. Natl. Acad. Sci. U.S.A. **78**, 3567 (1981).
11. J. Charvolin, J.-F. Sadoc, Biophys. Rev. Lett. **8**, 33 (2013).
12. G.C. Woods, M.K. Keech, Biochem. J. **75**, 588 (1960).
13. G.C. Woods, Biochem. J. **75**, 598 (1960).
14. G.C. Woods, Biochem. J. **75**, 605 (1960).
15. R.L. Trelstad, K. Hayashi, J. Gross, Proc. Natl. Acad. Sci. U.S.A. **73**, 4027 (1976).
16. R.R. Bruns, D.J.S. Hulmes, S.F. Terrien, J. Gross, Proc. Natl. Acad. Sci. U.S.A. **76**, 313 (1979).
17. D.J.S. Hulmes, R.R. Bruns, J. Gross, Proc. Natl. Acad. Sci. U.S.A. **80**, 388 (1983).
18. R.A. Gelman, B.R. Williams, K.A. Piez, J. Biol. Chem. **254**, 180 (1979).
19. D.E. Birk, E.I. Zycband, D.E. Winklemann, R.L. Trelstad, Proc. Natl. Acad. Sci. U.S.A. **86**, 4549 (1989).
20. K.E. Kadler, Y. Hojima, D.J. Prockop, Biochem. J. **268**, 339 (1990).
21. Nima Saedi, Thesis, *North Western University* (2009).
22. J.W. Weisel, C. Nagaswami, L. Makowski, Proc. Natl. Acad. Sci. U.S.A. **84**, 8991 (1987).
23. J. Charvolin, J.-F. Sadoc, Biophys. Rev. Lett. **9**, 225 (2014).
24. S. Cameron, L. Kreplak, A.D. Rutenberg, Soft Matter **14**, 4772 (2018).
25. G. Grason, Rev. Mod. Phys. **87**, 401 (2015).
26. K.E. Kadler, D.F. Holmes, J.A. Trotter, J.A. Chapman, Biochem. J. **316**, 1 (1996).
27. D.F. Holmes, J.A. Chapman, D.J. Prockop, K.E. Kadler, Proc. Natl. Acad. Sci. U.S.A. **89**, 9855 (1992).
28. D.J. Prockop, Fertala, J. Struct. Biol. **122**, 111 (1998).
29. A. Fertala, D.F. Holmes, K.E. Kadler, A.L. Sieron, J. Biol. Chem. **271**, 14864 (1996).
30. F.H. Silver, R.L. Trelstad, J. Biol. Chem. **255**, 9427 (1980).
31. J. Parkinson, K.E. Kadler, A. Brass, J. Mol. Biol. **247**, 823 (1994).
32. D. Silver, J. Miller, R. Harrison, D.J. Prockop, Proc. Natl. Acad. Sci. U.S.A. **89**, 9860 (1992).
33. I.N. Ridley, Math. Biosci. **58**, 129 (1982).
34. J.-F. Sadoc, N. Rivier, J. Charvolin, Acta Crystallogr. A **68**, 470 (2012).
35. S. Douady, Y. Couder, Phys. Rev. Lett. **68**, 2098 (1992).
36. N. Rivier, J.-F. Sadoc, J. Charvolin, Eur. Phys. J. E **39**, 7 (2016).
37. T. Gutsmann, G.E. Fantner, M. Venturoni, A. Ekani-Nikodo, J.B. Thompson, J.H. Kindt, D.E. Morse, D. Kuchnir Fygenso, P.K. Hansma, Biophys. J. **84**, 2593 (2003).
38. I.R. Bruss, G. Grason, Proc. Natl. Acad. Sci. U.S.A. **109**, 10781 (2012).
39. N. Rivier, J. Phys.: Condens. Matter **4**, 913 (1992).
40. S. Douady, Y. Couder, J. Theor. Biol. **178**, 255 (1996).
41. H.N. Yoshikawa, C. Mattis, P. Massia, G. Rousseaux, S. Douady, Eur. Phys. J. E **33**, 11 (2010).
42. J. Doucet, F. Briki, C. Pichon, L. Gumez, S. Bensamoun, J.-F. Sadoc, J. Struct. Biol. **173**, 197 (2011).
43. D.J. McBride, V. Choe, J.R. Shapiro, B. Brodsky, J. Mol. Biol. **270**, 275 (1997).
44. D.J.S. Hulmes, A. Miller, Nature **282**, 878 (1979).
45. J.P. Orgel, T.C. Irving, A. Miller, T.J. Wess, Proc. Natl. Acad. Sci. U.S.A. **103**, 9001 (2006).
46. V. Sasisekharan, M. Bansa, Curr. Sci. **59**, 863 (1990).